

Glassy dynamics of a kinetically constrained model: a direct comparison with experiment

M Jiménez-Ruiz^{1,8}, A Criado², F J Bermejo³, G J Cuello¹, F R Trouw⁴,
R Fernández-Perea³, H Löwen⁵, C Cabrillo⁶ and H E Fischer⁷

¹ Institut Laue-Langevin, BP 156x, F-38042 Grenoble Cedex 9, France

² Departamento de Física de la Materia Condensada, Universidad de Sevilla, PO Box 1065, E-41080 Seville, Spain

³ Consejo Superior de Investigaciones Científicas, Serrano 121-123, E-28006 Madrid, Spain

⁴ Los Alamos National Laboratory, MS H 805 LANSCE-12: LUJAN CENTER, Los Alamos, New Mexico 87545, USA

⁵ Institut für Theoretische Physik II, Heinrich-Heine-Universität, Universitätsstrasse 1, D-40225 Düsseldorf, Germany

⁶ Dept. Electricity and Electronics, Univ. Basque Country, PO Box 644, Bilbao E-48080, Spain

⁷ LURE, Bât 209D, Centre Universitaire, BP 34, 91898 Orsay Cedex, France

E-mail: jimenez@ill.fr

Received 3 December 2001

Published 7 February 2002

Online at stacks.iop.org/JPhysCM/14/1509

Abstract

The dynamics of the freezing transition of the rotator-phase crystal of ethanol into its orientational glass phase is monitored by measurements of molecular rotational components in the quasielastic neutron scattering spectrum. It is shown that phenomena experimentally observed at pico- and nanosecond scales can be mapped onto those shown by a model of infinitely thin hard needles rotating about body-centred cubic lattice positions. The basic signatures that appear on crossing the orientational glass transition are similar in the needle model and in the neutron scattering data for ethanol. As the model glass transition is of purely dynamical origin, our findings support the idea that the glass transition is purely dynamical and is not associated with an underlying thermodynamic phase transition.

1. Introduction

The nature of the non-equilibrium state produced by rapid cooling of a liquid, i.e. the canonical liquid–glass transition, remains an elusive question [1]. The transition may either be viewed as a purely dynamical phenomenon without any associated changes in static quantities [2] or as a remnant of an underlying thermodynamic phase change [3, 4] which is partially hidden for kinetic reasons. Arguments in favour of both points of view are partially supported by

⁸ Author to whom any correspondence should be addressed.

experimental data. On theoretical grounds, both alternatives have also been argued for, using either microscopic or thermodynamic approaches. Kinetic theories of the mode-coupling family [2] have been shown to have predictive capabilities concerning essential features of the micro- and mesoscopic dynamics of deeply supercooled liquids. In contrast, a variety of work carried out since the mid-1950s [5] at a phenomenological level has been able to rationalize a vast amount of experimental data. Most approaches are based upon thermodynamic concepts such as the ‘configurational entropy’ which should vanish at a temperature below the glass-transition temperature T_g in order to achieve consistency with the observed divergences of experimentally measurable quantities such as the dielectric relaxation time associated with the main peak of the dielectric susceptibility.

The main difficulties in evaluating the merits of both approaches concern the wide range of complex phenomena involved in the glass-transition of a real material, which can hide some of the features expected to appear as characteristic signatures of the transition. In fact, most systems where detailed studies can be carried out within the deeply supercooled liquid do show a rich variety of phenomena such as molecular rotations, i.e. involving *orientational degrees of freedom* (ODOF), and/or low-energy vibrations, which are strongly coupled to the translational dynamics due to the huge viscosity that is characteristic of temperatures near the glass-transition point T_g . This means that most experimental probes employed for the study of the dynamics may be sensitive to motion of the ODOF, while most theories deal with spherical objects executing translational motion only. While some progress has been made in understanding the effect of such motion on quantities usually employed to study the dynamic correlations at temperatures close to T_g [6], the question remains as to whether the structural liquid–glass transition is better understood as a purely dynamical phenomenon or as the result of the proximity of a random first-order transition as found in mean-field theories and density functional approaches [7].

The aim of this work is to test whether the glass transition leading from rotator-phase (RP) crystals to the orientationally disordered (orientational glass, OG) state can be understood as a purely dynamical crossover. In order to do so, we compare neutron scattering data for ethanol across the above-mentioned transition with that resulting from a simple, albeit non-trivial, model [8] which exhibits a purely dynamical crossover but has no static correlations. We find very similar signatures of the RP \rightarrow OG transition in both cases; this supports the idea that the transition is a purely dynamical phenomenon.

Our motivation for studying the RP \rightarrow OG transition on ethanol is threefold: first, while freezing of RP crystals has been studied in a fair number of systems, many details of the RP \rightarrow OG transition have been clarified recently for ethanol [9, 10]. Second, the presence of long-range positional periodicity on both sides of the RP \rightarrow OG transition implies that the melting process is purely rotational (rotation–translation coupling effects are reasonably small [11]), and can thus be followed by monitoring the neutron quasielastic scattering across the transition; this is in contrast with the canonical glass transition where the rotational melting is partially hidden by the emergence of quasielastic intensities from other sources. Third, ethyl alcohol has the unique feature that it can be prepared in two different phases showing glassy behaviour at the same temperature, one of these phases having structural disorder (liquid and glass) and the other having only orientational disorder (RP and OG). In the disordered crystals the molecular centres of mass sit at the nodes of a body-centred cubic (bcc) lattice [11, 12], and melting into the RP is signalled by jumps in specific heat [10] and thermal expansivity. The close proximity of both transitions was also revealed by dielectric spectroscopy [13] where both α - and sub- T_g relaxations appear astoundingly close in frequency- and temperature-dependence. Hence the canonical glass transition seems to be dominated by the freezing of the ODOF. If there is evidence that the RP \rightarrow OG transition is purely dynamical, the same

conclusion should apply for the canonical glass transition. Hence our study even sheds new light on the nature of the structural liquid–glass transition.

Last but not least, interest in clarifying the role of ODOF in glassy dynamics has very recently been reinvigorated by the finding of a linear term in the specific heat of ethanol below ≈ 1 K which is basically the same in both glassy phases [14]. In other words, the existence of an underlying lattice seems to have no effect on the characteristics of the two-level systems which drive the glassy dynamics within the fully quantum regime.

2. Experimental details

The measurements reported here are somewhat complementary to those already described involving macroscopic scales as explored by dielectric relaxation [13] and Brillouin light scattering [15, 16]. They were carried out using instruments with frequency windows around the meV range (to explore motions of the order of a picosecond) and around the μeV range (motions within the nanosecond scale). The instrument chosen to explore the former was the QENS inverted-geometry inelastic scattering spectrometer hosted by the IPNS (intense pulsed neutron source), while for the measurements carried out at μeV resolution the backscattering machine IN16 of the Institut Laue Langevin, Grenoble (France) was used. The achieved instrumental resolution at QENS was of the order of $90 \mu\text{eV}$ whereas that of IN16 was about 1 and $0.8 \mu\text{eV}$ for two different spectrometer settings, having energy transfer ranges up to ± 16 and $\pm 6 \mu\text{eV}$ respectively. Sample preparation and the general conditions of the experiment have been described a number of times [9, 10, 13] and basically involve annealing the deeply supercooled liquid until the strong (100) Bragg reflections of the bcc structure fully develop and no hint of the liquid main peak centred at $Q \approx 1.7 \text{ \AA}^{-1}$ remains in diffractograms collected at intervals of a few minutes. Fully deuterated ($\text{CD}_3\text{CD}_2\text{OD}$) and partially deuterated ($\text{CD}_3\text{CD}_2\text{OH}$) samples have been employed in the measurements. Although the presence of a sizeable coherent cross section complicates the analysis in terms of the simplest (incoherent) approximation, the use of partially deuterated samples is dictated by the need to monitor the state of the sample during annealing, which is done by direct inspection of the diffraction pattern.

Measurements carried out at QENS (upper frame) and IN16 (lower frame) revealed the presence of quasielastic broadening of the order of 0.3 meV and $4 \mu\text{eV}$ respectively as can be gauged from the spectra shown in figure 1. Spectra at a temperature below (left frame) and above (right frame) the glass transition for each instrument are shown in figure 1. A comparison of the spectra in the two columns shows that the increase in temperature leads to a concomitant increase in both quasielastic intensity and broadening.

Under the assumption that the movements within the two different frequency windows explored by the experiments correspond to just one kind of motion (which is supported by the results of computer simulations), the measured spectra were modelled in terms of an elastic δ -like peak plus a quasielastic component (convolved with the instrument resolution)

$$S(Q, \omega) = \left(\frac{I_{\text{quasi}}(Q)}{\pi} \frac{\Gamma(Q)/2}{\omega^2 + (\Gamma(Q)/2)^2} + I_{\text{el}}(Q)\delta(\omega) \right) \otimes R(Q, \omega) \quad (1)$$

where I_{el} and I_{quasi} are the elastic and quasielastic contributions respectively, $\Gamma/2$ is the quasielastic half-width and $R(Q, \omega)$ is the instrumental resolution.

It was found that the sets of data measured at both scales (μeV and meV) are affected by the finite range of achievable energy transfers, especially at the higher temperatures where the Lorentzian tails have not fully decayed. This would result in an underestimation of the linewidth which would become more severe as the temperature is increased. To remedy this, the experimental lineshapes were fitted introducing a constraint that accounts for the finite value of the maximum energy transfers. Details of the formal procedure of the fitting analysis can be found in [17]. The different contributions to the spectra are shown in figure 1.

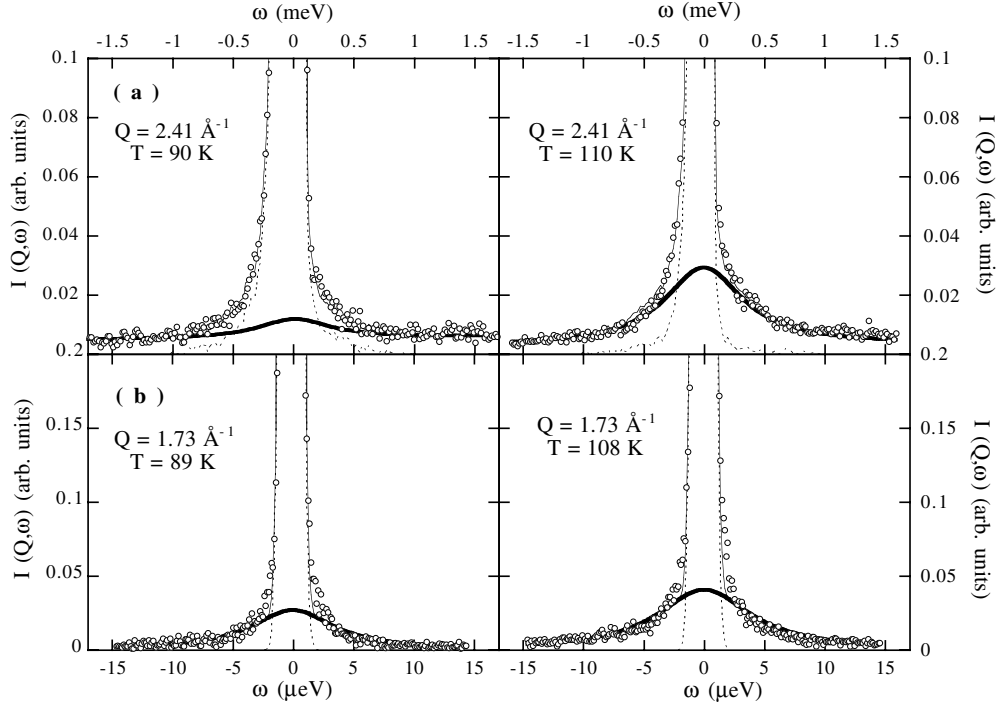


Figure 1. Spectra as measured on both QENS and IN16 spectrometers. Model fits are shown by thin solid curves. Dashed and thick full curves correspond to the elastic and quasielastic components respectively.

3. The hard needles model

In the quest for physically simple models which exhibit a purely dynamical glass transition, dense systems of compact impenetrable (hard) bodies are well known benchmarks where the rich physics of supercooled liquids can be investigated in great detail by means of computer simulations. For molecular materials, primitive models for such systems are derived by deformation of hard spheres towards hard ellipsoids of revolution. They are characterized by the diameter of the minor axes as well as the aspect ratio ℓ . The dynamics of a rotator crystal composed of such bodies is now starting to be investigated [18] within the context of the molecular mode coupling theory (MMCT). In the absence of a more realistic model we choose to compare our experimental results with those provided by a model of hard infinitely thin needles on a lattice as developed by Renner *et al* [8]. The system comprises a set of hard needles that have their centres of mass located at the sites of a cubic lattice and execute free rotations between elastic collisions. The only control parameter is the ratio $\ell = L/a$ of the needle length L to the lattice constant a [19]. Since the excluded volume of the needles is zero, all the static properties of the model are trivial (i.e. there are no static correlations). However, its transport and dynamical properties are highly non-trivial and exhibit a strong dependence on ℓ .

The dynamics of this a model is investigated by computer simulations. We consider a system of $N = 432$ infinitely thin needles with a homogeneous linear mass density m/L , whose centre of mass coordinates are fixed onto a bcc lattice in a periodically repeated cubic simulation box (figure 2). We took a bcc crystal in order to incorporate the ethanol lattice structure in the RP. The original algorithm employed by Renner *et al* [8] is employed for the

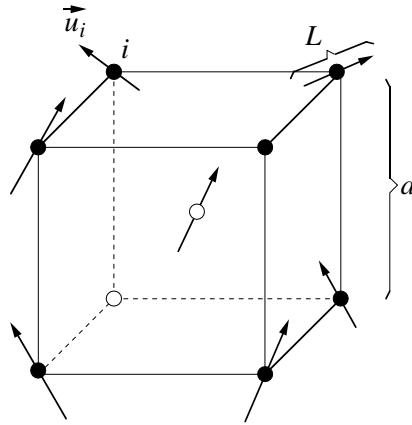


Figure 2. Unit cell of the system of hard needles sitting on the nodes of a bcc lattice.

calculation of the needle trajectories. It involves the solution of a transcendental equation at each simulation step, a process which becomes highly involved computationally for large values of ℓ .

From the calculated trajectories of the needles one calculates the time-autocorrelation function for the needle orientations defined as

$$\Phi_1(t) = \left\langle \frac{1}{N} \sum_{i=1}^N \vec{u}_i(0) \cdot \vec{u}_i(t) \right\rangle \quad (2)$$

where the angular brackets denote the canonical average and $\vec{u}_i(t)$ is the time-dependent trajectory of the unit vector describing the orientation of the i th needle. We explored the range $1.0 \leq \ell \leq 5.0$. The system was left to evolve over a long time corresponding to 10^6 collisions.

Figure 3 shows the time-autocorrelation function for different ratios of the needle length to the lattice parameter, $\ell = L/a$. As ℓ increases, the relaxation of $\Phi_1(t)$ becomes more and more sluggish, and for $\ell \sim 3.4$ the autocorrelation is almost blocked on the timescale explored in the simulation. For $\ell = 4.5$ the orientational autocorrelation is almost equal to unity which corresponds to orientations becoming frozen within a very narrow solid angle.

4. Experimental observations

The shape of all measured spectra conforms to that shown in figure 1. Both at meV and μeV scales it shows a strong elastic (resolution limited) component plus a quasielastic contribution which can be seen by the naked eye. A sample of the temperature dependence of the quasielastic linewidths for two representative values of the momentum transfer Q is shown in figure 4. No significant dependences were found for other explored Q values. Apart from details arising from the rather different frequency windows and scattering power of the two spectrometers, the same dependence is observed, showing that broadening of the quasielastic spectrum increases as the rotational melting transition is crossed.

The assignment of the observed broadenings to aspects of the underlying microscopic motion requires the use of a model to represent the dynamics. On symmetry grounds, one expects that its basic features are encompassed within a formalism describing molecular reorientations about the [100], [110] and [111] axes of a cubic lattice [20]. It predicts a neutron scattering law given in terms of four classes of molecular rotations with jump rates τ_j^{-1} ,

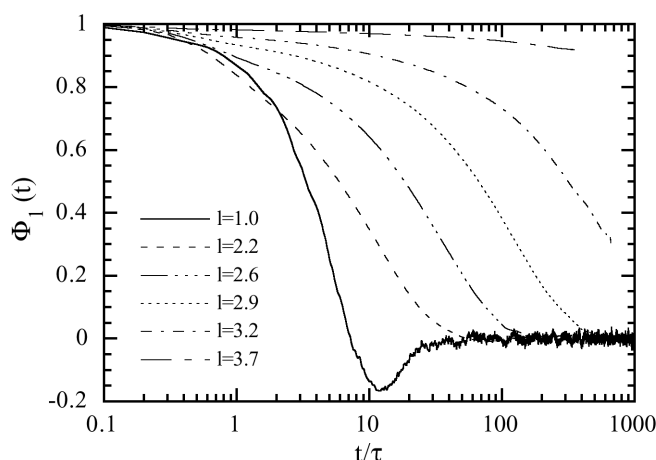


Figure 3. Orientational autocorrelation function $\Phi_1(t)$ versus reduced time t/τ for different ratios $\ell = L/a$.

$j = 1 \dots 4$. The timescale of two of these rates is set by the spectral linewidths measured with both instruments. However, their assignment to specific types of motion requires additional information from some other source. To this effect, we have carried out molecular dynamics simulations in the NPT ensemble (the cell shape is allowed to fluctuate) using a realistic model potential for the microscopic interactions [17]. The results of such an endeavour were gratifying, since (a) the equilibrium lattice structure is reproduced, (b) freezing of rotational motion occurs below 100 K and (c) the crystal structure becomes unstable above 120 K, which is quite close to the experimental value. From analysis of the computed trajectories, it was found that molecules will reorient between some 24 preferred orientations with vastly different rates. Reorientations leaving the most preferred orientations (C–O bond along the [001] direction and C–C bond close to $[11\bar{1}]$, and those related by symmetry) unaffected were found to take place within the picosecond scale, whereas far more infrequent jumps occurring within scales of hundreds of picosecond were also found. The calculated intermediate dynamic structure factor $F_{\text{MD}}(Q, t)$ showed strong deviations from exponential behaviour and, in fact, four different exponential decays were needed to fully account for its shape. The jump rates τ_j^{-1} estimated in this way were found to be well separated in time. Two of the decays were found to be within the frequency windows covered by the experiments and therefore we identify the observed relaxations with the two classes of motion described above.

Apart from the variation with temperature of the linewidth, the RP \rightarrow OG transition is also indicated by an increase with temperature of the quasielastic intensity and a concomitant decrease of the elastic peak, as can be seen in figure 5. In this figure the temperature dependences of the elastic and quasielastic intensities are shown, and as seen there the transition is nicely correlated with the transfer of spectral intensity from elastic to quasi- (or inelastic) scattering, showing very similar characteristics for both frequency windows (meV and μeV scales).

From the data given above it is seen that molecular rotations occur in the RP crystal on pico- and nanosecond scales at temperatures where the main α -relaxation explored by dielectric spectroscopy [13] already reaches macroscopic relaxation times. Well below 80 K rotational freezing seems complete, and all the molecular DOF which are thermally excited will contribute to the spectrum as inelastic (i.e. finite-frequency) signals [10]. This is in very good agreement with specific heat data [10] which also show that the extent in temperature of the transition is quite comparable with that shown by the present data (i.e. about 18 K).

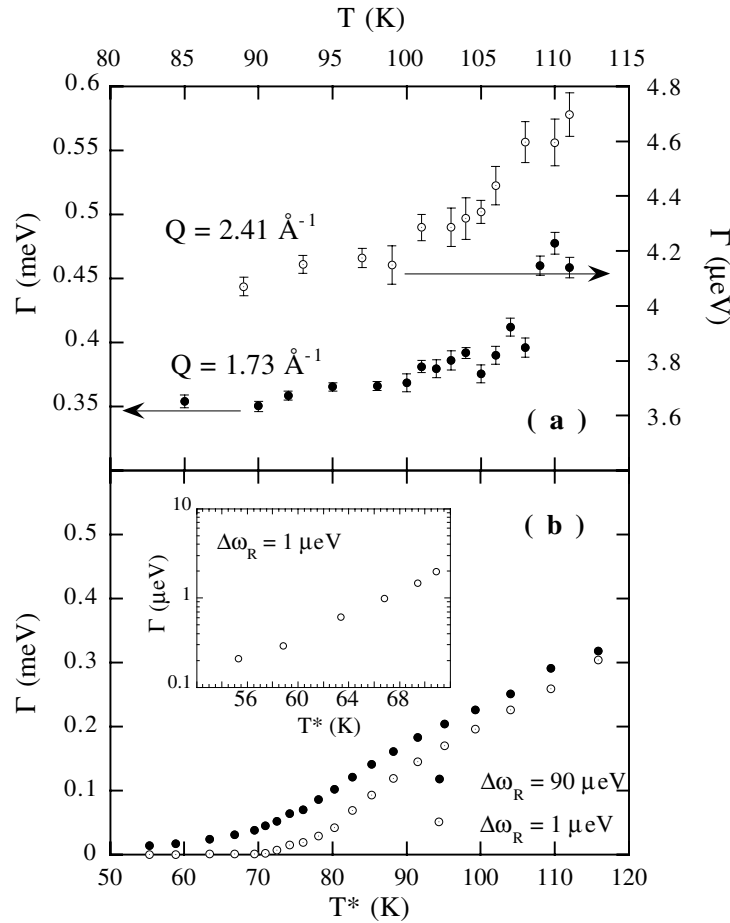


Figure 4. (a) Temperature dependence of the quasielastic linewidth as measured on the QENS (filled symbols) and IN16 (open symbols) spectrometers. (b) Variation of the width of $\Phi(\omega)$ as calculated from the results for a system of hard needles. The inset shows data in the μeV range on a semi-logarithmic plot.

5. Discussion: comparing the dynamics of hard needles with experiment

The first obvious difficulty in relating the results concerning the dynamics of hard needles to experiment regards the athermal nature of the model. In other words, one needs to establish a link between the control parameters of the simulation ($\ell = L/a$) and those of the experiment, i.e. the temperature.

5.1. Estimation of the microscopic timescale, τ

Since in the needle model the microscopic timescale is set by the time $\tau \equiv \sqrt{mL^2/24k_B T}$, the link between the ratio $\ell = L/a$ and the timescale is established directly. If we identify the moment of inertia of the needles $J = mL^2/12$ with the principal moment of inertia of an ethanol molecule ($J = 0.741 \times 10^{-45} \text{ kg m}^2$), we obtain that the timescale τ is of the order of 1 ps at $T = 100 \text{ K}$ and this sets the timescale.

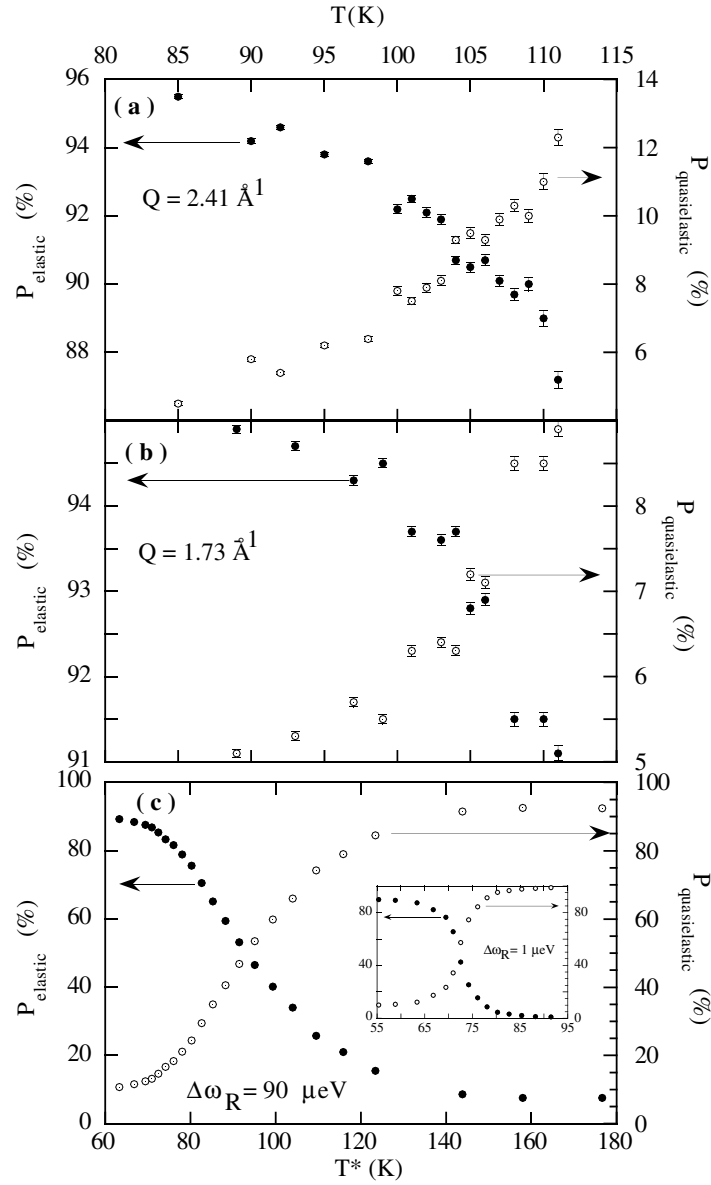


Figure 5. (a) Temperature dependence of the elastic (full symbols) and quasielastic (open symbols) intensities across the RP \rightarrow OG transition measured on the QENS spectrometer. (b) The same data measured on IN16. (c) Results from the hard needles model: contributions from $\Phi(\omega)$ to the elastic (solid) and quasielastic (open symbols) frequency windows, for the resolution width $\Delta\omega_R = 90 \text{ \mu eV}$, plotted against the equivalent temperature T^* . The inset shows data for the resolution width $\Delta\omega_R = 1 \text{ \mu eV}$.

5.2. Equivalent temperature of the simulation, T^*

In order to establish a mapping between ℓ and T , we start by considering the number of neighbours for one needle for which collisions are in principle possible as a ‘connectivity’

$$N_c \simeq \int dr^3 \rho \simeq \frac{4\pi}{3} L^3 \frac{2}{a^3} = \frac{8\pi}{3} \ell^3 \quad (3)$$

where the integral is to be taken over a sphere of radius L . One estimates that the inverse connectivity should be proportional to a Boltzmann factor, and since $N_c \propto \ell^3$ this leads us to define the inverse of the effective ratio $1/\ell$ as the Boltzmann factor⁸

$$1/\ell = A \exp(-E/k_B T). \quad (4)$$

Clearly the limit $\ell \rightarrow \infty$ corresponds to zero temperature. The two free constants, namely the amplitude A and the energy scale E , are determined as follows:

- (a) First we recall that if the needle length is smaller than the nearest neighbour distance $\sqrt{3}a/2$ the needles are non-interacting free rotators which corresponds to infinite temperature and sets the amplitude $A = 2/\sqrt{3} = 1/\ell_0$.
- (b) Second, the activation energy E should correspond to the experimental glass-transition temperature such that $E = k_B T_g$.

Taking into account these two conditions, the translation of temperatures in the experiment into effective ratios ℓ of our model is given by

$$\ell = \ell_0 \exp(T_g/T^*) \quad (5)$$

where $\ell_0 = \sqrt{3}/2$. With this relationship, and once the glass-transition temperature is known (in this case $T_g \sim 100$ K), all the simulation results can be shown as a function of the equivalent temperature T^* .

More refined mappings can also be justified. In particular, a nearly perfect match of the glass-transition temperatures of experiment and simulation is achieved if the characteristic energy is defined as $E = k_B T_g \ln[(8/3\sqrt{3})\ell_g]$ with ℓ_g being the aspect ratio at the midpoint of the freezing transition of the needle motion.

5.3. Comparison of the needle model with quasielastic neutron scattering results

To perform a meaningful comparison of experiment and model results one needs to follow the same steps. In other words one has to account for the finite instrumental resolution corresponding to both experiments. This has to be done by separating the spectrum into different contributions (elastic and quasielastic). This becomes a prerequisite since motions slower than a characteristic timescale for the lower-resolution instrument, QENS, will appear as a contribution to the elastic intensity on IN16, whereas fast motions detectable on QENS will only contribute as a flat background on the higher-resolution instrument, IN16.

5.3.1. Choice of the resolution function $F_{\text{res}}(t)$. As explained above, the experiments on quasielastic neutron scattering were carried out using two different instruments, QENS and IN16, having very different instrumental resolutions. This means that the choice of the resolution function must be made depending on the frequency scale considered. The resolution functions for both instruments show a lineshape close to a Lorentzian function in frequency space which gives rise to exponential functions in the temporal representation

$$F_{\text{res}}(t) = e^{-t/\tau} \quad (6)$$

or

$$\mathcal{F}(F_{\text{res}}(t)) = \tilde{F}_{\text{res}}(\omega) = \frac{\Delta\omega_R}{\omega^2 + \Delta\omega_R^2}. \quad (7)$$

With these equations F_{res} is determined from the half-width of the measured instrumental response functions (these quantities are available from the instrument characteristics), and the relevant figures are given below.

⁸ A more elaborate mapping is known for hard spheres where the effective diameter is also taken as an averaged Boltzmann factor in order to match the second virial coefficient, see e.g. [21].

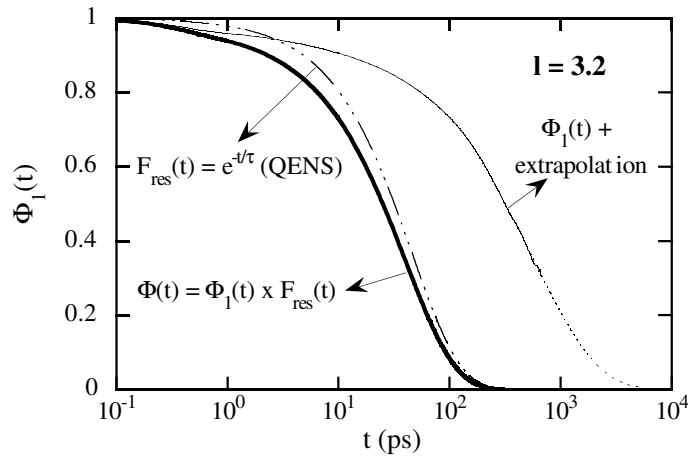


Figure 6. Graphical representation of the steps followed in order to compare the needle model results for $\ell = 3.2$ with the quasielastic neutron scattering results measured in QENS. First, the resolution function $F_{\text{res}}(t)$ is obtained, secondly $\Phi_1(t)$ is extrapolated and finally $\Phi(t)$ is obtained as the product of these two functions (which corresponds to the convolution of $\tilde{F}_{\text{res}}(\omega)$ and $\tilde{\Phi}_1(\omega)$).

5.3.2. Extrapolation of $\Phi_1(t)$ to long times. As shown in figure 3, for values of $\ell = 2.9$ and above the autocorrelation function has not decayed completely in the available time window. So in order to perform Fourier transforms which avoid high-frequency truncation ripples, the function $\Phi_1(t)$ was extrapolated to long times with the von Schweidler function [2]. Choosing a different extrapolation scheme such as the Kolrausch law gave rather similar results. Before separating the different contributions of the spectrum (elastic and quasielastic) it was necessary to convolve $\Phi_1(t)$ with the experimental resolution.

5.3.3. Convolution with the experimental resolution. In order to perform the convolution we use the following property: if

$$\tilde{F}_{\text{res}} = \int_0^{\infty} e^{-i\omega t} F_{\text{res}}(t) dt \quad (8)$$

and

$$\tilde{\Phi}_1(\omega) = \int_0^{\infty} e^{-i\omega t} \Phi_1(t) dt \quad (9)$$

are the Fourier transforms of $F_{\text{res}}(t)$ and $\Phi_1(t)$ respectively, then the Fourier transform of $F_{\text{res}}(t) \times \Phi_1(t)$ is the convolution of $\tilde{F}_{\text{res}}(\omega)$ and $\tilde{\Phi}_1(\omega)$. Taking into account that the resolution functions are exponentials with time decays given in table 1 and in order to simplify the analysis, we introduce the new function $\Phi(t)$

$$\Phi(t) = \Phi_1(t)e^{-t/\tau}. \quad (10)$$

An example of the steps followed is provided in figure 6 which shows data for $\ell = 3.2$ compared with results measured on QENS.

5.3.4. Separation of the different contributions. The Fourier transform of $\Phi(t)$, denoted by $\Phi(\omega)$, can now be split into elastic and quasielastic contributions depending upon the experimental resolution $\Delta\omega_R$ affecting the target experimental data. As pointed out above, the

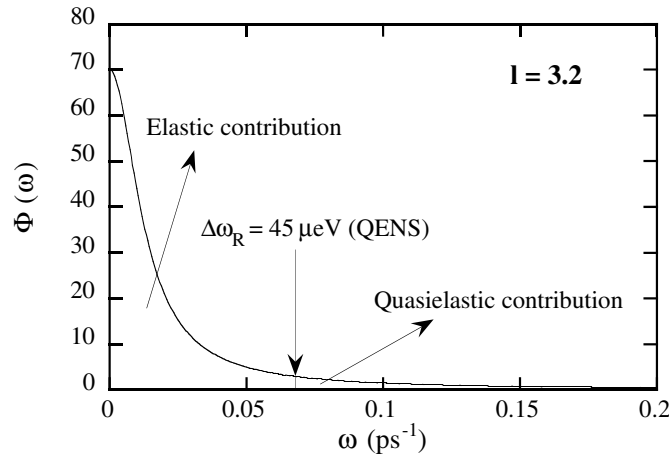


Figure 7. Fourier transformation of $\Phi(t)$, $\Phi(\omega)$, with the elastic and quasielastic contributions. The arrow shows the resolution of the QENS spectrometer.

Table 1. Values of the experimental resolution.

Instrument	$\Delta\omega_R$ (HWHM) (μeV)	τ (ps)
QENS	45	91.9
IN16	0.5	8271.3

elastic contribution was considered as the contribution to $\Phi(\omega)$ from frequencies below the resolution, and the quasielastic one as the contribution from frequencies above (figure 7).

The width and the amplitude of the quasielastic part were determined afterwards. The results for the widths are given in figure 4 and those for the intensity ratios in figure 5. Note that the simulation data are always expressed in terms of temperature via the translation given above. One clearly sees a kink in the quasielastic intensity (a change in slope) both in the experimental data and in the transformed needle model data. This kink is observed at temperatures of about 97 K for the experimental results (figures 5(a) and (b)) and of about 75 K for the ones from the model (figure 5(c)). This is a clearcut fingerprint of the orientational glass transition. As is expected, since the total intensity must be constant (100%), the elastic intensity exhibits a similar kink. The differences between experiment and model concern the relative magnitudes of changes in elastic and quasielastic intensities as well as the absolute values of the linewidths. Whereas the experiment contains a strong elastic scattering component arising from the presence of a well defined crystal structure having translational DOF, such a contribution is obviously absent in the model which, by construction, shows no strictly elastic component. The relative widths of the crossovers are about 30 K in the experiments and ≈ 70 K for the needle model, a difference expected from the absence in the latter case of a true interaction potential. The effective widths of the quasielastic spectra of both model and experiment shown in figure 4 exhibit crossovers at the same temperatures where the kinks in the intensities appear in figure 5. This provides compelling evidence that the essential signatures of the orientational glass transition can be understood from a purely dynamical model.

6. Conclusions

In conclusion, we have shown that the essential features of the neutron scattering data near the orientational glass transition can be understood in terms of a purely dynamical phenomenon. The fingerprints of the transition as revealed by a kink in the inelastic scattering are very similar in the experiment and in the model. The implications of such an analogy in dynamical behaviour can, in the light of previous data, to a large extent be applied to the canonical glass/liquid transition, inasmuch as the latter must carry a large rotational component (in fact, the jump in specific heat at the glass and OG \rightarrow RP transitions corresponds to an activation of ≈ 2.8 DOF in the latter and about 3.7 in the former, the extra degree surely assignable to translational motions). In consequence, the scenario of a transition of purely dynamical origin accounts for most of the observed signatures of the glass transition which, put into real numbers, amounts to a difference of about 20% of the jump in specific heat, an even smaller difference in the low-frequency spectra and low-temperature properties, and a close proximity in the case of macroscopic relaxations.

Finally, the results described in this paper are also consistent with the recent simulation data reported by Affouard and Descamps [22] for a primitive model of chloroadamantane, another orientationally disordered crystal. Their results indicate behaviour which seems to conform to predictions made on the basis of the idealized version of the mode-coupling theory.

Acknowledgments

Work supported in part by the US Department of Energy, Basic Energy Sciences–Materials Sciences, under Contract W-31-109-ENG-38 and DGICYT (Spain) grant no PB98-0673-c02-01.

References

- [1] Gutzow I and Schmelzer J 1995 *The Vitreous State* (Berlin: Springer) p 287
- [2] Götze W 1991 *Liquids, Freezing and Glass Transition* ed J P Hansen *et al* (Amsterdam: North-Holland)
Götze W 1999 *J. Phys.: Condens. Matter* **11** A1
- [3] Sethna J P, Shore J D and Huang M 1991 *Phys. Rev. B* **44** 4943
- [4] Bletry J 1996 *Z. Naturf. A* **51** 87
- [5] Adam G and Gibbs J H 1965 *J. Chem. Phys.* **43** 139
Bestul A B and Chang S S 1994 *J. Chem. Phys.* **40** 3731
Xia X and Wolynes P G 2001 *Phys. Rev. Lett.* **86** 5526
- [6] Schilling R and Scheidsteger T 1997 *Phys. Rev. E* **56** 2932
Winkler A *et al* 2000 *Phys. Rev. E* **62** 8004
Theenhaus T *et al* 2001 *Preprint cond-mat/0105393*
- [7] Mezard M and Parisi G 1999 *Phys. Rev. Lett.* **82** 747
Dasgupta C and Valls O T 1999 *Phys. Rev. E* **59** 3123
- [8] Renner C, Löwen H and Barrat J L 1995 *Phys. Rev. E* **52** 5091
Obukhov S, Kobzeb D, Perchak D and Rubinstein M 1997 *J. Phys. I France* **7** 563
- [9] Ramos M A, Vieira S, Bermejo J F, Dawidowski J, Fischer H E, Schober H, González M A, Loong C K and Price D L 1997 *Phys. Rev. Lett.* **78** 82
- [10] Talón C, Ramos M A, Vieira S, Cuello G J, Bermejo F J, Criado A, Senent M L, Bennington S M, Fischer H E and Schober H 1998 *Phys. Rev. B* **58** 745
- [11] Bermejo F J, Criado A, Fayos R, Fernández-Perea, Fischer H E, Suard E, Guelylah A and Zúñiga J 1997 *Phys. Rev. B* **56** 11 536
- [12] Fayos R, Bermejo F J, Dawidowski F J, Fischer H E and González M A 1996 *Phys. Rev. Lett.* **77** 3823
- [13] Miller M, Jiménez-Ruiz M, Bermejo F J and Birge N O 1998 *Phys. Rev. B* **57** R13 977
Jiménez-Ruiz M, González M A, Bermejo F J, Miller M A, Birge N O, Cendoya I and Alegría A 1999 *Phys. Rev. B* **59** 9155

- [14] Talón C, Ramos M A, Vieira S, Shmytko I, Afonikova N, Criado A, Madariaga G and Bermejo F J 2001 *J. Non-Cryst. Solids* **287** 226
- [15] Criado A, Jiménez-Ruiz M, Cabrillo C, Bermejo F J, Grimsditch M, Fischer H E, Bennington S M and Eccleston R S 2000 *Phys. Rev. B* **61** 8778
- [16] Fischer H E, Bermejo F J, Cuello G J, Fernández-Díaz, Dawidowski J, González M A, Schober H and Jiménez-Ruiz M 1999 *Phys. Rev. Lett.* **82** 1193
- [17] Criado A, Jiménez-Ruiz M, Cabrillo C, Bermejo F J, Fernández-Perea R, Fischer H E and Trouw F R 2000 *Phys. Rev. B* **61** 12082
- [18] Schilling R 2001 Private communication
- [19] Frenkel D and Maguire J F 1981 *Phys. Rev. Lett.* **47** 1025
Frenkel D and Maguire J F 1983 *Mol. Phys.* **49** 503
- [20] Bée M 1988 *Quasielastic Neutron Scattering* (Bristol: Adam Hilger) p 228
- [21] Barker J A and Henderson D 1976 *Rev. Mod. Phys.* **48** 587
- [22] Affouard F and Descamps M 2001 *Phys. Rev. Lett.* **87** 35 501